Commun. Comput. Phys.
doi: 10.4208/cicp.2009.09.025

Vol. **7**, No. 3, pp. 597-612
March 2010

Multi-Scale Modeling and Numerical Simulation for CVI Process

Yun Bai[1], Xingye Yue[1,*] and Qingfeng Zeng[2]

[1] *Department of Mathematics, University of Science and Technology of China, Hefei, Anhui, 230026, China.*
[2] *National Key Laboratory of Thermostructure Composite Materials, Northwestern Polytechnical University, Xi-an, 710072, China.*

Received 31 January 2009; Accepted (in revised version) 13 July 2009

Communicated by Pingwen Zhang

Available online 9 October 2009

Abstract. We consider the multi-scale modeling of the isothermal chemical vapor infiltration (CVI) process for the fabrication of C/SiC composites. We first present a microscopic model in which the preform is regarded as a two-phase porous media described by a dynamic pore-scale node-bond network during the fabrication process. We then develop a macroscopic model by a upscaling procedure based on the homogenization theory.

AMS subject classifications: 65M60

Key words: Multiscale modeling, composite materials, two-phase porous media, node-bond network, homogenization.

1 Introduction

1.1 Background

The CVI process is the chemical vapor infiltration process which is widely used in fabrication of ceramic matrix composite materials (CMCs). One important kind of CMCs is the carbon fiber reinforced silicon carbide (C/SiC) composites. The principal of CVI process is that let the agent gases pass through the reactor, and when the agent gases reach the surface of the carbon fiber, surface reaction happens and SiC solid is generated and deposited. When almost all the pores in the preform are occluded, we derive the material of carbon fiber reinforced SiC. One point to be noted is the multi-scale structure

*Corresponding author. *Email addresses:* by1900@mail.ustc.edu.cn (Y. Bai), xyyue@ustc.edu.cn (X. Yue), qfzeng@nwpu.edu.cn (Q. Zeng)

 ©2010 Global-Science Press

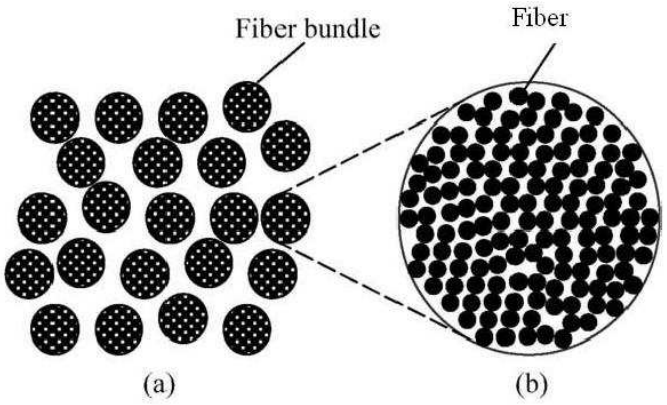

Figure 1: (a) Cross section perpendicular to randomly positioned bundles; (b) Cross section perpendicular to randomly positioned fibers inside a fiber bundle.

of the preform. A preform can have hundreds of fiber bundles or more woven together. A fiber bundle has several thousands of fibers inside. There are two kinds of pores in the preform: macro pores among bundles and micro pores among fibers inside the bundles as in Fig. 1 [16]. In the cross section of a preform, the diameter of the micro pores is in the magnitude order of μm, the diameter of the macro pores is in the magnitude order of mm and the size of a preform can be several centimeters or larger. During the numerical simulation, if we simply use the traditional numerical tools like Finite Element Method or Finite Difference Method on this multi-scale structure, a huge amount of computer memory and CPU time are required, which can easily beyond the limit of the computing resources. Some macroscale models have been developed to simulate this process, see, e.g., [9, 10, 16, 17, 19]. However, there are problems remained in these models which will be presented in Section 1.2. So a new multiscale model is proposed in this paper.

1.2 Classical model

In the last twenty years, many works are related to the modeling of the CVI process. The main model used in those works, e.g., in [13–17], will be described below.

Assume the chemical reaction in the preform is the following:

$$\mathrm{MTS}(\mathrm{CH_3SiCl_{3(v)}}) \xrightarrow{\text{excess } H_2} \mathrm{SiC_{(s)}} + 3\mathrm{HCl_{(v)}}. \tag{1.1}$$

1.2.1 Concentration equation

Assume the mass transfer in the CVI process is quasi-steady, i.e.,

$$\frac{dC}{dt} = 0.$$

Then the concentration equation can be written out as

$$-\nabla\cdot(D_{eff}\nabla C)=R, \tag{1.2}$$

where C is the molarity of MTS (mol/m^3), D_{eff} is the effective diffusion coefficient of MTS. Because the deposition reaction of MTS is regarded as first order, the reaction term R can be given as

$$R=-KCS_v,$$

where K is the first-order surface reaction rate constant (m/s), and S_v is the effective deposition surface area per unit volume (m^2/m^3).

1.2.2 Diffusion model

In the classical models the effective diffusion coefficient is proportional to porosity and inversely proportional to a structural parameter of the preform, the tortuosity factor:

$$D_{eff}=\frac{\varepsilon}{\tau}D, \tag{1.3}$$

where

$$\tau=\frac{\tau_0\varepsilon_0}{\varepsilon},$$

τ_0 is the initial tortuosity factor, ε is the porosity of the preform and ε_0 is the initial porosity. The diffusion coefficient D is the mixed diffusion coefficient which is described in the following form

$$\frac{1}{D}=\frac{1}{D_{AB}}+\frac{1}{D_K}, \tag{1.4}$$

where D_{AB} is the Fick diffusion coefficient (m^2/s) which can be estimated from the Chapman-Enskog theory [1]. Fick diffusion happens when the diameter of the diffusion tunnel is much larger than the molecular mean free path and is mainly caused by the molecular transport. D_K is the Knudsen diffusion coefficient given by

$$D_K=\frac{2}{3}\left(\frac{8\bar{R}T}{\pi M}\right)^{1/2}r_s, \tag{1.5}$$

where $\bar{R}$ is the gas constant $(J/K/mol)$, $T(K)$ is the temperature, M is the molecular weight of the diffusion gas, and r_s is the mean radius of the diffusion tunnel.

Knudsen diffusion happens when the diameter of the diffusion tunnel is smaller than the molecular mean free path and is dominated by the collision between molecular and tunnel wall. The change of r_s during the CVI process is estimated using the formula

$$\frac{dr_s}{dt}=-q\frac{M_{SiC}}{\rho}KC, \tag{1.6}$$

where q is the proportion between the stoichiometric coefficient of SiC and that of MTS in Eq. (1.1), and M_{SiC} is the molar mass of SiC (kg/mol).

In the CVI process, the Knudsen diffusion has significant effect on the gas diffusion in micro pores among fibers and less effect on the gas diffusion in macro pores among bundles.

1.2.3 Evolution equation of porosity

The evolution equation of local porosity in CVI process can be written as:

$$\begin{cases} \dfrac{d\phi}{dt} = -q\dfrac{M_{SiC}}{\rho} S_v K C, & t>0, \\ \phi = \phi_0, & t=0, \end{cases} \tag{1.7}$$

where ρ is the density of SiC (kg m^{-3}), ϕ_0 the initial porosity of the preform, and S_v the effective deposition surface area per unit volume (m^2/m^3).

By calculating the porosity, the procedure of CVI process can be tracked. When the porosity ε is sufficiently small, the CVI process terminates.

1.2.4 Discussion about classical model

The classical model can describe the change of the pore structure during the CVI process. However, there are problems in this model.

The preform has the multi-scale pore structure. The micro pores inside the fiber filaments are much smaller than the macro pores among fiber bundles. During the CVI process, in the initial stage, the deposition mainly happens in the micro pores. After the micro pores are almost closed, the deposition will turn to happen in the macro pores. At this point, only Fick diffusion happens in the macro pores and the Knudsen diffusion coefficient $D_K \approx 0$. Then by (1.4) we have $D \approx 0$, i.e., the effective diffusion coefficient $D_{eff} \approx 0$. This result contradicts the real experiments. The whole CVI process may last for several hundreds of hours, and the initial stage only last for tens of hours. After the initial stage, the diffusion rate in the preform is determined by the size of macro pores. So the effective diffusion coefficient can not tend to 0 at the initial tens of hours. To avoid this, some simulations choose the r_s in (1.6) as the average radius of all the pores in the preform so it will not quickly decrease to 0. But this approach is unreasonable. Another problem is that the classical models only involve the overall porosity to track the CVI process which cannot naturally distinguish the two different deposition stages, i.e., we can not tell when the micro pores in the bundles is closed. So some modified models should be investigated to fix the problems for the classical models.

2 A revised model

To avoid the problems in the classical macroscopic model, we first go back to see what happens in a 'microscopic' scale. At first, we need to make some basic **Assumptions:**

- H1: Fiber bundle fraction all over the preform before infiltration is uniform and the preform is considered as isotropy.
- H2: The macro pore structure of the preform is periodic before infiltration and locally periodic during all the CVI process.
- H3: The micro pore structure inside fiber bundle is uniformly distributed during all the CVI process.
- H4: Chemical reaction is regarded as an isothermal irreversible first-order reaction.

2.1 Micro model

2.1.1 Deal with multi-scale structure

The diffusion types in the macro pores and micro pores are different. So the preform can be viewed as a material with two different phases. Phase I is the fiber bundles, which consists of fibers and micro pores among fibers, and Phase II is the macro pores among bundles.

Phase I is regarded as a homogeneous porous material. Define the diffusion coefficient D_1 in Phase I as:

$$D_1=\begin{cases} \phi_{sb}\, D_{AB} & : \quad r_s \geq r_0, \\ \phi_{sb}\, D_K & : \quad r_s \leq r_0,\ \phi_{sb} > \phi_{sc}, \\ 0 & : \quad \phi_{sb} \leq \phi_{sc}. \end{cases} \tag{2.1}$$

If the micro pore radius r_s is smaller than the molecular mean free path r_0,the diffusion type is the Knudson diffusion. In (2.1), ϕ_{sb} is the porosity of the micro pores inside fiber bundle defined as following:

$$\phi_{sb}=\frac{\text{volume of micro pores in a fiber bundle}}{\text{volume of the fiber bundle}};$$

ϕ_{sc} is the critical (residual) porosity of the micro pores inside fiber bundle, under which the micro pores will be closed.

Diffusion in Phase II, D_2 is the Fick diffusion D_{AB} at the beginning of the CVI process. As chemical reaction happens, the radius r_l of macro pores will decrease. Near the end of the reaction process, r_l may be smaller than the molecular mean free path r_0, and the diffusion type will change to Knudson diffusion, i.e.,

$$D_2=\begin{cases} D_{AB} & : \quad r_l \geq r_0, \\ D_K & : \quad r_l < r_0. \end{cases} \tag{2.2}$$

During the CVI process, surface reaction happens and more and more SiC solid is generated and deposited. So the structure of the micro and macro pores change all the

way. We assume that the radius of micro pores in the same fiber bundle decrease uniformly but the decrease rate may be different at different bundles in the preform and assume that the shrink direction of the macro pores be along the outer normal of their surface and the rate be determined by the generation rate of the deposited solid.

2.1.2 Reaction-diffusion equation

Based on the above process, the preform includes two scales. The characteristic size at microscale is the scale of a macro pore. With this point of view, the preform is regarded as heterogenous porous media. The macroscale is the scale of the whole preform. At this scale, the preform is viewed as a homogeneous material.

First, certain geometry model needs to be used to describe the initial shape and structure of the preform, like the location of the macro pores and fiber bundles. Based on this model, we introduce the character function $\chi(x,\frac{x}{\epsilon},t)$ to depict the structure of the preform, which is defined as

$$\chi\Big(x,\frac{x}{\epsilon},t\Big)=\begin{cases}1, & x \text{ in macro pores},\\ 0, & \text{otherwise}.\end{cases} \tag{2.3}$$

According to the mass conservation, in micro-scale the quasi-steady reaction diffusion equation can be written as

$$-\nabla\cdot(D^{\epsilon}\nabla C)+R^{\epsilon}=0. \tag{2.4}$$

At different place diffusion situation is different, so the diffusion coefficient D^{ϵ} is a function of $x=(x_1,x_2,x_3)$, defined as

$$D^{\epsilon}:=D\Big(x,\frac{x}{\epsilon},t\Big)=D_1\Big(1-\chi(x,\frac{x}{\epsilon},t)\Big)+D_2\chi\Big(x,\frac{x}{\epsilon},t\Big). \tag{2.5}$$

At the beginning the structure of the preform is assumed to be periodic. As the reaction happens and the solid generates, the inside structure of the preform will change and as a result its micro structure is no longer periodic. But we can still assume the structure is locally periodic (Assumption H2). ϵ can be chosen as the initial period of the preform structure which is of the same order of magnitude as the characteristic diameter of the macro pore. According to the structure of the preform, the characteristic function and D^{ϵ} should be locally periodic with period ϵ.

Assume the reaction is first order so only surface reaction is considered. We also regard Phase I as a homogeneous porous material. So the reaction term can be written as

$$R^{\epsilon}=KC\delta_l(x,t)+KCS_{vs}\Big(1-\chi(x,\frac{x}{\epsilon},t)\Big), \tag{2.6}$$

where $\delta_l(x,t)$ is the surface dirac delta function defined as

$$\int_{\Omega}\delta(x,t)f(x,t)dx=\int_{S_l}fds,$$

for any smooth function $f(x,t)$ and S_l is the surface of the macro pores. The S_{vs} is the effective deposition surface area of micro pores in Phase I defined as

$$S_{vs}=\frac{\text{surface of micro pores in a fiber bundle}}{\text{volume of the fiber bundle}}\cdot\Big(\frac{\phi_{sb}-\phi_{sc}}{\phi_{sb0}-\phi_{sc}}\Big)^{\gamma},\quad 0<\gamma\leq 1, \tag{2.7}$$

when the micro porosity is above its critical point $\phi_{sb}>\phi_{sc}$, otherwise the effective deposition surface area is set to be zero $S_{vs}=0$. ϕ_{sb0} is the initial porosity of micro pores in a fiber bundle. Note that some part of the micro pores may have been closed above the critical porosity ϕ_{sc}, so we introduce the term $(\frac{\phi_{sb}-\phi_{sc}}{\phi_{sb0}-\phi_{sc}})^{\gamma}$ to control the decrease of the effective deposition area.

In (2.6), we simply divide the reaction term into two parts according to the preform structure characteristic. The first term $KC\delta_l(x,t)$ is the reaction on the surface of the macro pores. The second term $KCS_{vs}(1-\chi(x,\frac{x}{\epsilon},t))$ is the surface reaction in Phase I. This separation enables us to know (1) how much solid is deposited on the surface of macro pores and then how the macro pore structure changes; and (2) how much solid is deposited in phase I and then the corresponding D_1 and S_{vs}.

However, the time cost for solving this problem in the micro view is tremendous especially when the preform domain is large, the pore structure of the preform is complicated, and the reaction time is quite long. So we have to sacrifice some details to save our computational cost. In other words, the micro-problem should be converted to macro-scale.

2.2 Macro-model

2.2.1 Macro molarity equation

We follow the step in the homogenization theory [7] to solve the periodic problem. Let $y=x/\epsilon$ be the fast variable and x the slow variable. Consequently, $C(x,\frac{x}{\epsilon},t)=C(x,y,t)$.

The homogenized molarity equation with the quasi-steady assumption can be written out: Find $C^0=C^0(x,t)$ such that

$$-\nabla_x\cdot(D_{eff}(x,t)\nabla_x C^0)=-R, \tag{2.8}$$

$$D_{eff}(x,t)=<D(x,y,t)(I+\nabla_y N(x,y,t))>, \tag{2.9}$$

where $y=\frac{x}{\epsilon},D(x,y,t)=D(x,\frac{x}{\epsilon},t)=D^{\epsilon}$ and the average symbol $<.>$ is defined as

$$<\cdot>=\frac{1}{|\square|}\int_{\square}\cdot\quad dy, \tag{2.10}$$

where $\square$ is the unit cube $[0,1]^3$ which is a period cell, and $|\square|$ is the volume of $\square$. In (2.8), $N=N(x,y,t)=(N_1,N_2,N_3)$ is a vector periodic function about y, which satisfies the following cell problem:

$$-\nabla_y\cdot(D(x,y,t)\nabla_y N)=\nabla_y\cdot D(x,y,t),\ \ y\in\square, \tag{2.11a}$$

$$N \text{ is } \square \text{ periodic about } y, \text{ and } \int_Y N dy=0. \tag{2.11b}$$

The right-hand side term R of (2.8) is the macro reaction term, which has the form

$$R = KS_{vl}C^0(x,t) + KS_{vs}(1-\phi_l)C^0(x,t), \tag{2.12}$$

where S_{vl} is the effective deposition surface area of macro pores per unit volume and ϕ_l the porosity of macro pores among fiber bundles.

Remark 2.1. It can be proved that the micro reaction term R^ϵ converges to the macro reaction term R when ϵ tends to zero, though the original reaction term R^ϵ is singular due to the existence of the surface dirac delta function. Actually, for a simplified linear micro model:

$$-\nabla\cdot\left(D(x,\frac{x}{\epsilon})\nabla C\right) = -KC\delta_l(x) - KCS_{vs}\left(1-\chi(x,\frac{x}{\epsilon})\right) \quad \text{in } \Omega, \tag{2.13a}$$

$$C = \tilde{C} \quad \text{on } \partial\Omega, \tag{2.13b}$$

its corresponding macro model is

$$-\nabla_x\cdot\left(D_{eff}(x)\nabla_x C^0\right) = -KC^0(x)S_{vl} - KS_{vs}C^0(x)(1-\phi_l) \quad \text{in } \Omega, \tag{2.14a}$$

$$C = \tilde{C} \quad \text{on } \partial\Omega. \tag{2.14b}$$

By the homogenization theory, we can derive the following error estimate under H^1 norm:

$$\|C - (C^0 + \epsilon N(x,y)\cdot\nabla C^0)\|_1 \le A\sqrt{\epsilon},$$

where A is a constant independent of ϵ. The key point is to prove the convergence of the singular reaction term $KC\delta_l(x)$ to $KC^0(x)S_{vl}$. This can be achieved by an observation that the term $\int_{S_l} KC^0 w ds$, where S_l is the collection of all macro pore surface, is in some sense a 'numerical quadrature' of $\int_\Omega KS_{vl}C^0 w dx$ for any proper test function w. The detail of its proof and the proof of the convergence for the real micro model leave to the future work.

2.2.2 Porosity evolution

The overall porosity ϕ can also be divided into two parts naturally, ϕ_l the porosity of macro pores among fiber bundles and ϕ_s the porosity of micro pores in the bundles. So $\phi = \phi_l + \phi_s$. Base on (2.12), rewrite the porosity evolution equations:

$$\frac{d\phi_s}{dt} = -q\frac{M_{SiC}}{\rho_{SiC}}S_{vs}(1-\phi_l)KC^0, \tag{2.15}$$

$$\frac{d\phi_l}{dt} = -q\frac{M_{SiC}}{\rho_{SiC}}S_{vl}KC^0. \tag{2.16}$$

Note that the surface of macro pores (i.e., the surface of fiber bundles) actually consists of the surface of fibers lying on the outer boundary of fiber bundles (see Fig. 1), which is only a small part of all fibers. So at the initial stage the micro pores provide most

deposition surface (i.e., the surface of all fibers inside the bundles) and its total area is larger than the area of the surface of macro pores for several magnitudes. So the chemical deposition almost happens in micro pores. As a result, the porosity of the micro pores decreases very quickly at this stage, but the macro pores change a little. After the micro pores are almost closed, i.e., there exists a critical porosity ϕ_{sc} when $\phi_s \leq \phi_{sc}$, the chemical deposition does not happen in the micro pores any longer and so that in the later stage only the porosity of macro pores decrease. At this moment, $S_{vs} = 0$. Eq. (2.16) is not calculated and D_1 the diffusion coefficient in Phase I is set to be zero in (2.5).

Remark 2.2. When micro pores are closed, the diffusion coefficient in Phase I is $D_1 = 0$. At this moment, the effective diffusion coefficient in (2.9) does not equal to 0, which is different from the classical model. The dominant part in the effective diffusion coefficient is the diffusion in the macro pores.

Remark 2.3. By Eqs. (2.15) and (2.16), the volume of the solid deposited in the macro pores and Phase I can be calculated separately. Therefore, we can detect the structure of the macro pores change and calculate the character radius r_s of micro pores. Consequently, the calculation for D_{eff} based on Eqs. (2.9) and (2.11) can be realized as the pore structure change. More importantly, we can clearly monitor the time when the micro pores are almost closed.

3 Numerical simulation and results

3.1 Numerical simulation

3.1.1 Domain description and pore structure modeling

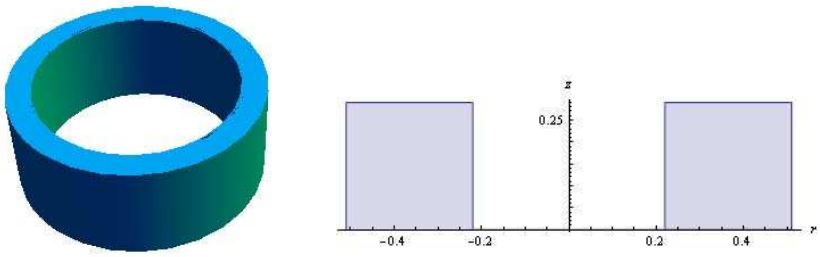

(a) 3-D display (b) Cross section

Figure 2: The preform.

The initial preform shown in Fig. 2 is a cylinder with the wall thickness 28.5745 cm and height 28.5745 cm. Set up cylinder coordinates (r,θ,z) on this preform and make the preform to be axis symmetric. The intersection of the preform in the r-z plane is shown contains 1000 fiber bundles. Assume the reactor is also cylinder and axis symmetric. Consequently, we only need to solve a 2-D problem here.

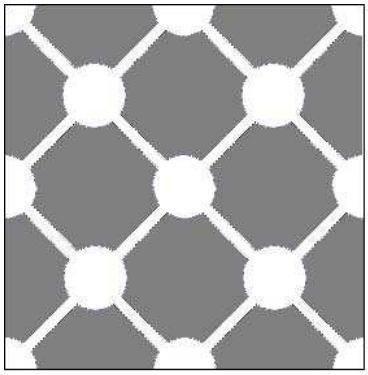

Figure 3: Node-Bond model.

We need to introduce pore structure to simulate the pore shape and distribution in the preform so that we can locate the initial position where the deposition happens. There are a lot of models to simulate the pore structure, including single pore model [6, 12], the parallel bundle model [14, 15], the overlap model [3, 11] and the node-bond network model [13]. However, most models deal with single scale pore. So for this multi-scale problem, we need to combine different models together to solve our problem. Considering the periodic structure of the initial preform, we follow the method in [16, 17] by choosing node-bond network model in Fig. 3 to simulate the fibre bundle and macro pore distribution in the preform. The grey part is fibre bundles and white part is macro pores. For the micro pores inside the fibre bundle, we assume they are uniformly circle.

As the reaction happens, the radius of micro pores in the same fiber bundle decrease uniformly but the decrease rate may be different at different bundles in the preform. The shrink direction of the macro pores is along the outer normal of their surface and the rate is determined by the generation rate of the deposited solid.

The effective deposition surface area of macro pores can be estimated as following:

$$S_{vl} = \frac{\text{surface of large pores in node-bond model}}{\text{total area}}. \tag{3.1}$$

3.1.2 Molarity equation

According to homogenization theory and the assumption of axis symmetry, we have the homogenized molarity equation in the cylinder coordinate:

$$\begin{aligned} &D_{11}\Big(\frac{\partial^2 C^0(r,z)}{\partial r^2}+\frac{1}{r}\frac{\partial C^0(r,z)}{\partial r}\Big)+D_{12}\frac{\partial^2 C^0(r,z)}{\partial r\partial z}+D_{21}\Big(\frac{1}{r}\frac{\partial C^0(r,z)}{\partial z}+\frac{\partial^2 C^0(r,z)}{\partial z\partial r}\Big)\\ &\quad+D_{22}\frac{\partial^2 C^0(r,z)}{\partial z^2}=-\Big(KS_{vl}C^0(r,z)+KS_{vs}(1-\phi_l)C^0(r,z)\Big), \end{aligned} \tag{3.2}$$

where (r,z) are slow variable and $\bar{r},\bar{z}$ are fast variables, defined as $\bar{r}=r/\epsilon$, $\bar{z}=z/\epsilon$, and

$$D(r,z,\bar{r},\bar{z},t)=D_1(1-\chi(r,z,\bar{r},\bar{z},t))+D_2\chi(r,z,\bar{r},\bar{z},t), \tag{3.3a}$$

$$D_{11}=\left\langle D(r,z,\bar{r},\bar{z})(1+\frac{\partial N_1(\bar{r},\bar{z})}{\partial \bar{r}})\right\rangle,\quad D_{12}=\left\langle D(r,z,\bar{r},\bar{z})\frac{\partial N_1(\bar{r},\bar{z})}{\partial \bar{z}}\right\rangle, \tag{3.3b}$$

$$D_{21}=\left\langle D(r,z,\bar{r},\bar{z})\frac{\partial N_2(\bar{r},\bar{z})}{\partial \bar{r}}\right\rangle,\quad D_{22}=\left\langle D(r,z,\bar{r},\bar{z})(1+\frac{\partial N_2(\bar{r},\bar{z})}{\partial \bar{z}})\right\rangle. \tag{3.3c}$$

In (3.3), $<\cdot>$ is defined by (2.10), $\square\in\mathcal{R}^2$ is the unit square, $N_1(\bar{r},\bar{z})$ and $N_2(\bar{r},\bar{z})$ satisfy the auxiliary problems:

$$\begin{cases} \frac{\partial}{\partial \bar{r}}\left(D\frac{\partial N_1}{\partial \bar{r}}\right)+\frac{\partial}{\partial \bar{z}}\left(D\frac{\partial N_1}{\partial \bar{z}}\right)=-\frac{\partial D}{\partial \bar{r}}, & \text{in } \square,\\ \frac{\partial}{\partial \bar{r}}\left(D\frac{\partial N_2}{\partial \bar{r}}\right)+\frac{\partial}{\partial \bar{z}}\left(D\frac{\partial N_2}{\partial \bar{z}}\right)=-\frac{\partial D}{\partial \bar{z}}, & \text{in } \square,\\ N_1(\bar{r},\bar{z}),N_2(\bar{r},\bar{z}) \text{ is periodic about } (\bar{r},\bar{z}). \end{cases} \tag{3.4}$$

3.1.3 Implementation

Table 1 shows the data for implementation.

Table 1: Area 28.5745×28.5745 (mm^2) $\gamma=0.5$.

Parameter	Value
D_b, radius of bond	0.01571(mm)
L_b, length of bond	0.16923 (mm)
R_n, radius of node	0.07324 (mm)
R_f, radius of a fiber bundle	0.3 (mm)
ϕ_{s0}, initial porosity of micro pores	0.3336
ϕ_{l0}, initial porosity of macro pores	0.2224
ϕ_0, initial porosity of preform	0.556

The computational domain is divided into 16×16 elements, the coarse mesh. Each element contains 4×4 cells, see Fig. 4. The 16 cells inside an element assume to be periodic, and the pore structure in different elements may be different as the chemical deposition happens. The substructure of a cell is node-bond pore structure. The computation process of each time step is following:

1. Solve auxiliary problem (3.4) on a sample cell with fine mesh in each element. Then the effective diffusion coefficient on each element can be obtained by (3.3).
2. Solve the macro concentration equation (3.2) on the coarse mesh.
3. Solve the porosity evolution equations (2.15) and (2.16) on the coarse mesh.
4. According to the current porosity, calculate the volume change of the macro pores and micro pores and then determine the new node-bond structure and calculate the current radius of node and bond, r_s, S_{vl} and S_{vs}.
5. Computation ends when the porosity of the macro pores is small enough. If computation does not end, return to step 1 for next time step.

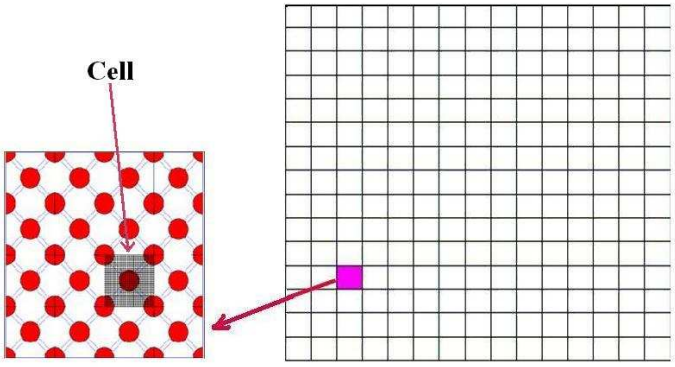

Figure 4: Macro mesh, node-bond structure and local cell.

Remark 3.1. The algorithm above falls into the framework of Heterogeneous Multiscale Methods (see [4, 5]), for we estimate the macro data D_{eff} for the macro model though solving the local cell problems in micro scale. Its complexity is independent of the characteristic size of the macro pore structure ε. When the assumption (H2) is false, i.e., pore structure is not initially periodic or not locally periodic during the CVI process, our algorithm will also work, if we could properly choose the local sample cells instead of the period cell used here, see [18] for the principle of choosing the local samples.

3.2 Result and analysis

Numerical experiments are carried out to simulate the chemical experiment under $1000^{\circ}C$ and 0.05 atm. Fig. 5 shows the porosity distribution of Phase I at the initial stage. At the center of the preform, the agent gases diffuse slower than at the boundary so that the chemical deposition is constrained at the center. Porosity change at the center is slower than at the boundary. So the porosity at the center is larger than that the boundary.

Fig. 6 is the concentration distribution at later stage when chemical deposition happens in the macro pores. The concentration gradient still exists because of the diffusion and keeps increase as the pores getting smaller. Fig. 7 is the porosity of the preform at later stage. The change of porosity gets slower at this stage than the initial stage. At this stage, chemical reaction is less than at the initial stage because most micro pores which provide quite a lot deposition surface are closed so the chemical deposition only happens on the surface of macro pores which is quite less than that the micro pores can provide.

In Fig. 8, the change of concentration in the center of the preform with time is clear. It should be noted that the profile of concentration first decrease then increase, and then decrease again. The first decrease is caused by the fast chemical reaction at the beginning. As micro pores are gradually closed, the reaction term $KS_{vs}(1-\phi_l)$ decreases fast but the diffusion does not decrease too much so diffusion begins to be dominant, which causes the increase in the profile. The second decrease is caused by the close process of the macro pores. At this stage the diffusion which is mainly decided by the size of macro

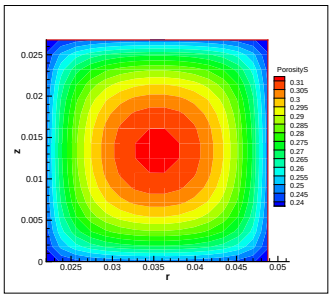

(a) $t=9$ hours.

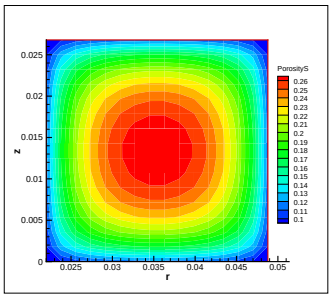

(b) $t=27$ hours.

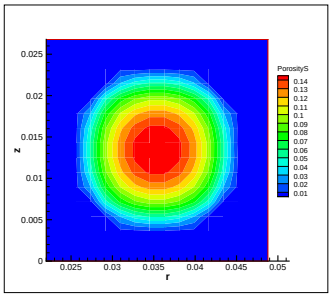

(c) $t=63$ hours.

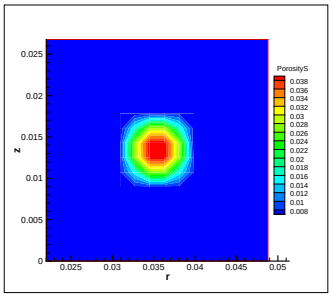

(d) $t=130$ hours.

Figure 5: Porosity of Phase I distribution at initial stage.

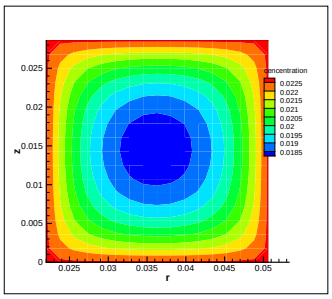

(a) $t=240$ hours.

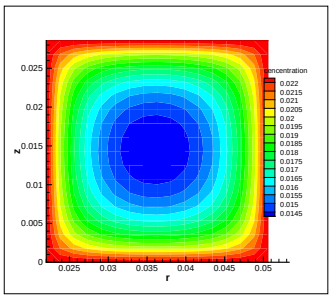

(b) $t=300$ hours.

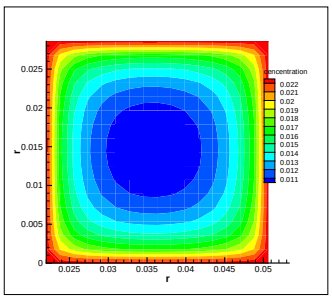

(c) $t=380$ hours.

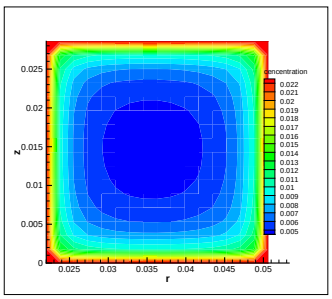

(d) $t=490$ hours.

Figure 6: Concentration distribution at later stage.

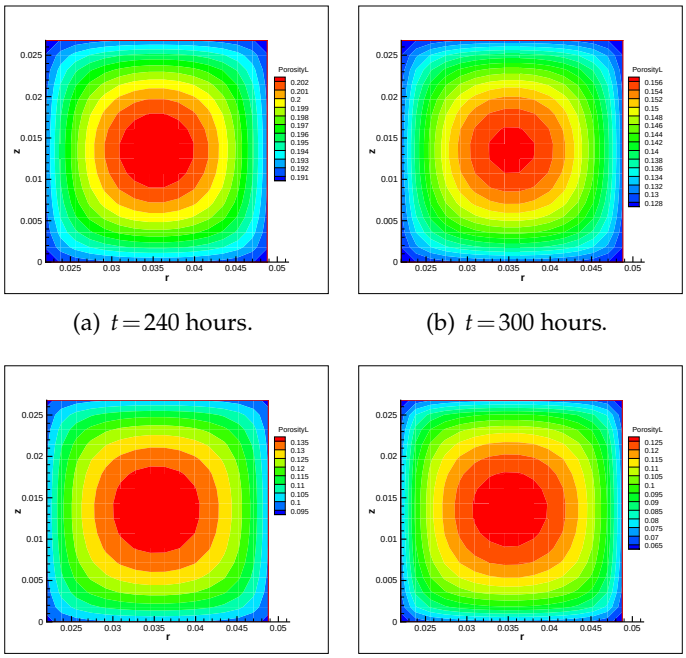

(a) $t=240$ hours. (b) $t=300$ hours.

(c) $t=380$ hours. (d) $t=490$ hours.

Figure 7: Porosity of macro pores distribution at later stage.

pores decreases so the concentration at the center goes down again. This result matches the real experiment better and is similar to the result described in [2] which exploits the pore model with micro pores and macro pores. If the micro and macro pores are not considered separately, this result will not be shown. Fig. 9 shows the porosity change of macro pores and micro pores with time. In the initial stage, the porosity of micro pores quickly decrease to its critical point (i.e., residual porosity), and the porosity of macro pores changes slowly. After the micro pores are almost closed, the concentration of MTS inside the preform increases because of the sharp decrease of the effective deposition area and large pressure outside the preform, so that the porosity of macro pores begins to decrease more quickly in the later stage.

4 Conclusion

We developed a multi-scale model for the isothermal chemical vapor infiltration (CVI) process for the fabrication of C/SiC composites, which fixed some drawbacks of the existing macroscopic models. However, we still need some ad hoc assumptions and inputs, such as the local periodic Assumption (H2), the critical porosity ϕ_{sc}, and the parameter γ in (2.1) and (2.7). Furthermore, the residual pore structure in the composite affects the properties of the material. Our model can not predict the residual pore structure correctly

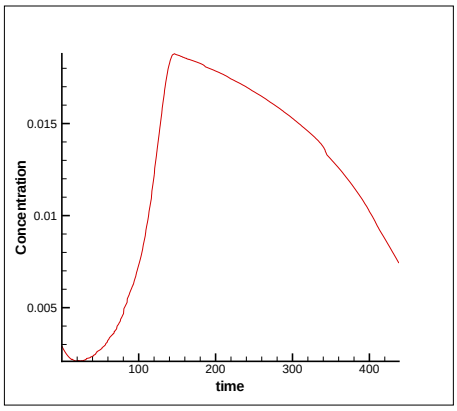

Figure 8: The change of concentration in the center of the preform with time.

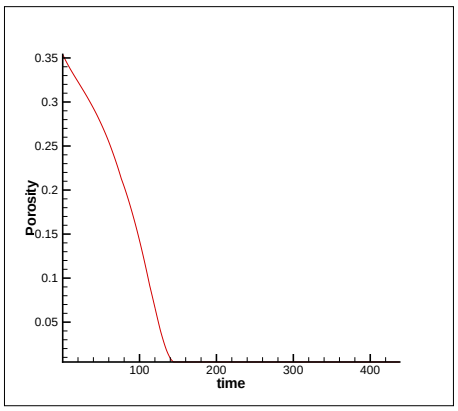

(a) Porosity of micro pores.

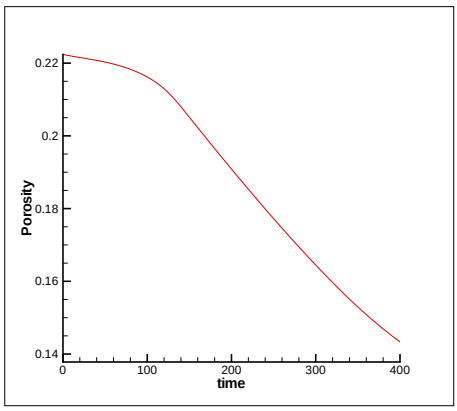

(b) Porosity of macro pores.

Figure 9: The change of porosity in the center of the preform with time.

yet. We plan to construct a macro-micro coupling model. MTS concentration evolves in macro scale, while the pore structure evolution in the local cells (samples) will be simulated directly in micro scale by, e.g., level-set method [8]. Simulations on these local samples will yield not only the macroscopic parameter such as effective diffusion coefficient, effective reaction surface area and porosity of macro pores, but also the statistic for the residual pore structure.

Acknowledgments

We benefitted a great deal from discussions with Prof. Shi Jin of the University of Wisconsin. The work of Yue is supported in part by NSF of China under the grant 10871190 and the National Basic Research Program under the Grant 2005CB321704. The work of Zeng is supported in part by Flying Star Program of Northwestern Polytechnical University and NSF of China under the Grant 50802076.

References

[1] R.B. Bird, W.E. Stewart and E.N. Lightfoot, Transport Phenomena, John Wiley and Sons, New York, 1960.
[2] G.Y. Chung and B.J. McCoy, Modeling of chemical vapor infiltration for ceramic composites reinforced with layered, woven fabrics. J. Am. Ceram. Soc., 74(4) (1991), 746-751.
[3] R.P. Currier, Overlap model for chemical vapor infiltration of carbon in porous carbon substrates. J. Am. Ceram. Soc., 73(8) (1990), 2274-2280.
[4] W. E and B. Engquist, The heterogeneous multiscale methods. Commun. Math. Sci., 1 (2003), 87-132.
[5] W. E, B. Engquist, X. Li, W. Ren and E. Vanden-Eijnden, Heterogeneous multiscale methods: A review. Commun. Comput. Phys., 2 (2007), 367-450.
[6] F. Erich and G. Ranier, Fiber-reinforced silicon carbidge. American Ceramic Society Bulletin, 65(2) (1986), 326-335.
[7] V.V.Jikov, O.A.Oleinik and S.M.Kozlov, Homogenization of Differential Operators and Integral Functionals. Springer-Verlag, 1994.
[8] S. Jin, X. Wang, T.L. Starr and X.F. Chen, Robust numerical simulation of porosity evolution in chemical vapor infiltration. I: Two space dimension. J. Comput. Phys., 162 (2000), 467-482.
[9] G.Q. Lu, Modelling the densification of porous structures in CVI ceramic composites processing. J. Mas. Proc. Tech., 37 (1993), 487-498.
[10] B.W. Shenldon and T.M. Besmann, Reaction and diffusion kinetics during the initial stages of isothermal chemical vapor infiltration. J. Am. Ceram. Soc., 74(12) (1991), 3046-3053.
[11] P. McAllister and E.E. Wolff, Modelling of chemical vapor infiltration of carbon in porous carbon substrates. Carbon, 29(4) (1991), 387-396.
[12] M. Middleman, B. Heble and H.C.T. Cheng, Improved uniformity of densification of ceramic composites through control of the initial preform porosity distribution. J. Mater. Res., 5 (1990), 1544-1548.
[13] T.L. Starr, Gas transport model for chemical vapor infiltration. J. Mater. Res., 10(9) (1995), 2360-2366.
[14] N.H. Tai and T.W. Chou, Analytical modeling of chemical vapor infiltration in fabrication of ceramic composites. J. Am. Ceram. Soc., 72(3) (1989), 414-420.
[15] N.H. Tai and T.W. Chou, Modeling of an improved chemical vapor infiltration process for ceramic composites fabrication. J. Am. Ceram. Soc., 73(6) (1990), 1489-1498.
[16] X. Wei, L.F. Cheng, L.T. Zhang and Y.D. Xu, A two-dimensional model for densification behavior of C/SiC composites in isothermal chemical vapor infiltration. Modelling Simul. Mater. Sci. Eng., 14 (2006), 891-904.
[17] X. Wei, L.F. Cheng, L.T. Zhang, Y.D. Xu and Q.F. Zeng, Numerical simulation for fabrication of C/SiC composites in isothermal CVI reactor. Computational Materials Science, 38(2) (2006), 245-255.
[18] X. Yue and W. E, The local microscale problem in the multiscale modeling of strongly heterogeneous media: effects of boundary conditions and cell size. J. Comput. Phys., 222 (2007), 556-572.
[19] Q.F. Zeng, Optimization design for C/SiC composites (in Chinese). PhD Thesis, Northwestern Polytechnical University, 2004.